Cellular and Molecular Life Sciences (2025) 82:203
https://doi.org/10.1007/s00018-025-05726-5

ORIGINAL ARTICLE

Downregulation of CMIP contributes to preeclampsia development by impairing trophoblast function via the PDE7B-cAMP pathway

Yina Li[1,2] · Xinjing Yan[1,3] · Haiyang Yu[1,2] · Yuanbo Zhou[1,2] · Yongrui Gao[1,2] · Xinyuan Zhou[1,4] · Yujie Yuan[1] · Yangnan Ding[1,2] · Qianqian Shi[1,2] · Yang Fang[1,2] · Hongmei Du[1,2] · Enwu Yuan[1,2,5] · Xin Zhao[5,6] · Linlin Zhang[1,2,5]

Received: 20 January 2025 / Revised: 24 April 2025 / Accepted: 24 April 2025

Abstract

Background Preeclampsia (PE) is one of the leading causes of perinatal maternal and fetal morbidity and mortality, but its precise mechanism remains elusive. Previous research has suggested that c-Maf-inducible protein (CMIP) is abnormally expressed in PE pathophysiology. Therefore, we aimed to explore the potential role of CMIP and its downstream molecules in PE.

Methods Multiplex immunofluorescence and immunohistochemical assays were conducted on preeclamptic placentas. Functional analysis of CMIP was performed in HTR-8/SVneo cells through transfection experiments in which either CMIP was overexpressed or downregulated. RNA sequencing was utilized to identify the molecular pathways downstream of CMIP. The impact of hypoxia on CMIP levels was assessed in three different types of trophoblast cells. The therapeutic efficacy of CMIP was evaluated in an N(ω)-nitro-L-arginine methyl ester (L-NAME)-induced rat model of PE.

Results CMIP expression was downregulated in extrachorionic trophoblasts (EVTs) and syncytiotrophoblasts (STBs) in preeclamptic placentas. This downregulation of CMIP in trophoblast cells disrupts cell proliferation, migration, invasion, and angiogenesis by upregulating the PDE7B-cAMP pathway, while elevated CMIP levels enhance these cellular functions. Hypoxia reduced CMIP expression in all three types of trophoblast cells. Moreover, in a rat model of PE, supplementation with CMIP alleviated hypertension and increased fetal weight and number.

Conclusions Our study demonstrates for the first time that the CMIP-PDE7B-cAMP pathway contributes to PE development by influencing trophoblast function. The signaling pathway proteins involved in PE induced by CMIP may provide new clues to the occurrence of PE and new targets for future PE therapy.

Yina Li, Xinjing Yan and Haiyang Yu contributed equally to this article.

✉ Xin Zhao
zdsfyzx@zzu.edu.cn

✉ Linlin Zhang
zll7376@zzu.edu.cn

[1] Department of Laboratory Medicine, Third Affiliated Hospital of Zhengzhou University, 7 Kangfu Qian Street, Zhengzhou, Henan 450052, People's Republic of China

[2] Zhengzhou Key Laboratory for In Vitro Diagnosis of Hypertensive Disorders of Pregnancy, Zhengzhou, China

[3] Department of Blood Transfusion, Xi'an People's Hospital, Xi'an 710000, China

[4] Department of Obstetrics and Gynecology, The Third Affiliated Hospital of Zhengzhou University, Zhengzhou, China

[5] Tianjian Advanced Biomedical Laboratory, Zhengzhou, China

[6] Radiology Department, Third Affiliated Hospital of Zhengzhou University, 7 Kangfu Qian Street, Zhengzhou, Henan 450052, People's Republic of China

Published online: 15 May 2025

Graphical Abstract

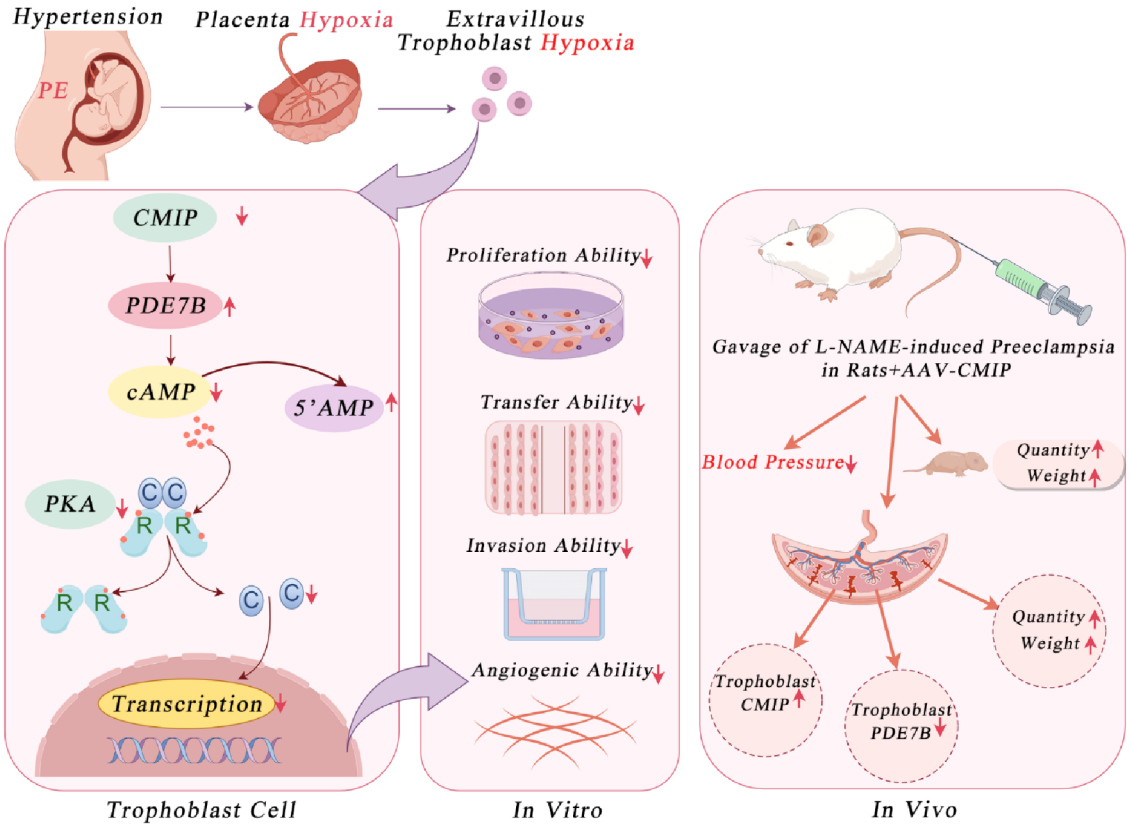

Keywords CMIP · PDE7B · cAMP · Trophoblast cells · Preeclampsia

Abbreviations

PE	Preeclampsia
NP	Normal pregnancy
EVT	Extravillous trophoblast
STB	Syncytiotrophoblast
CMIP	C-Maf-inducing protein
cAMP	Cyclic adenosine monophosphate
PKA	Protein kinase A
L-NAME	N(ω)-nitro-L-arginine methyl ester
eNOS	Endothelial nitric oxide synthase
NO	Nitric oxide

Introduction

PE is a common disease characterized by abrupt onset hypertension, proteinuria, and end-organ dysfunction after 20 weeks of pregnancy. Maternal morbidity and mortality from PE have increased globally in recent years and typically affect 2-5% of pregnancies [1, 2]. However, therapeutic options remain limited, and symptoms are primarily relieved by placental delivery, which frequently results in preterm labor and poses significant risks to maternal and fetal health [3].

PE is a disease affecting the placenta, a short-lived functional organ that connects the mother and fetus. Impaired placental function caused by insufficient proliferation, migration, and invasion of trophoblasts, as well as the failure of spiral artery remodeling, is recognized as a critical cause of PE [3]. Although aberrant trophoblast function has been linked to PE, the specific signaling pathways that are implicated in this disease remain an active area of research. The signaling pathways currently known to be involved in PE include the PI3K/AKT, mTOR, WNT, and NF-κB pathways [4–7]. Despite advances in understanding these pathways, therapeutic interventions have not yet achieved complete symptom relief or disease prevention, suggesting that additional factors regulating trophoblast function may play critical roles and warrant further investigation.

CMIP may be one of the factors influencing trophoblast function. Our preliminary study and two others revealed that CMIP is abnormally expressed in the placentas of PE patients, suggesting its possible involvement in the pathophysiology of the disease. However, the exact mechanism

of CMIP involvement in PE remains unknown [8–10]. The CMIP gene, located on chromosome 16q24, encodes CMIP, a multifunctional junction protein that has been found to play various roles in different signaling pathways [11, 12]. Studies have demonstrated that CMIP inhibits Fyn kinase activity in podocytes via disruption of the Csk-Fyn-Akt signaling axis, thereby impairing nephrin phosphorylation [13, 14]. CMIP also acts as a negative regulator of T-cell activity [15]. Additionally, CMIP is expressed in several types of cancers, including Hodgkin's lymphoma [16], gastrointestinal tubular adenocarcinoma [17], gliomas [18], and triple-negative breast malignancies [19]. In these cancers, CMIP promotes cancer cell proliferation and migration, which are associated with poor prognosis [12]. Given that CMIP has been shown to play diverse roles in different cell types, such as inhibiting Fyn family members in podocytes, regulating T-cell activity, and promoting cancer cell proliferation in various malignancies, it is likely that the downstream pathways mediated by CMIP vary depending on the cellular context. In trophoblast cells, CMIP may modulate their functions through a novel pathway. Further research is needed to fully understand the role of CMIP in trophoblast cells and its implications for cellular functions.

Therefore, the objective of this study was to investigate the localization and expression levels of CMIP in both normal and preeclamptic placental tissues, examine its impact on trophoblast function and associated signaling pathways, and determine its potential role in the pathogenesis of preeclampsia.

Materials and methods

Human placental tissues

Subjects were recruited from the Third Affiliated Hospital of Zhengzhou University from July 2023 to October 2024 and were divided into two groups: preeclampsia (PE, $n=20$) and normal pregnancy (NP, $n=20$) groups. PE was diagnosed according to the criteria of the American Congress of Obstetricians and Gynecologists [3]. Women who delivered at or after 37 weeks of gestation without complications during pregnancy were included in the NP group. The inclusion and exclusion criteria, as well as the placental collection methods, were based on previous studies [6]. The tissues were washed with cold phosphate-buffered saline(PBS) to remove maternal and fetal blood. The placental tissues used for wax block embedding were stored in 4% paraformaldehyde fixative (G1101, Servicebio). Maternal samples were collected for immunohistochemistry and immunofluorescence studies. The baseline characteristics of the included clinical subjects are presented in Supplementary Table 3. The human study was approved by the Human Research Ethics Board of the Third Affiliated Hospital of Zhengzhou University, and informed consent was obtained from all participants prior to enrollment. The ethics approval reference number was 2022-338-01.

Histopathological analysis

Multiplex fluorescence immunohistochemical staining: Human placental tissues were collected and fixed in 4% paraformaldehyde. After the tissues were embedded in paraffin, the samples were sectioned into 2–5 μm-thick slices. The sections were dewaxed and antigenically repaired. Citric acid repair solution (pH 6.0) was boiled under high pressure and added to the sectioning frame. The lid was tightly covered for 2 min, the heating was stopped, and the temperature was lowered by rinsing with tap water until it cooled. The lid was then opened and removed.

The sections were subsequently treated with antigen retrieval buffer (G1202-250ML, Servicebio) and 3% hydrogen peroxide at room temperature for 25 min in the dark. Subsequently, 3% bovine serum albumin(BSA) (Servicebio) was applied to the slides, which were subsequently sealed and incubated at room temperature for 30 min. The slides were incubated overnight at 4 °C with primary antibodies, followed by three washes with PBS (pH 7.4) (G0002, Servicebio). The following primary antibodies were used: anti-CMIP, anti-PDE7B, and anti-human leukocyte antigen-G(anti-HLA-G).

The slides were incubated with secondary antibodies corresponding to the primary antibody at room temperature for 50 min. The following secondary antibody was used: HRP-labeled goat anti-rabbit IgG secondary antibody. After the slides were washed three times with PBS, they were exposed to iF555-tyramide (1:500, G1233, Servicebio), iF488-tyramide (1:500, G1231, Servicebio), or iF647-tyramide (1:500, G1232, Servicebio) and incubated at room temperature in the dark for 10 min. The slides were rinsed three times with PBS. The tissue sections were placed in a repair cassette filled with a pH 6.0 citric acid repair solution (G1202, Servicebio) and heated in a microwave oven to maintain boiling for approximately 10 min to remove the primary and secondary antibodies bound to the tissues. The above steps were repeated twice to complete the process of staining a slide with the three antibodies, and finally, the slide was laid flat in a lightproof wet box (SIB-20 F, Servicebio). 4',6-Diamidino-2-phenylindole(DAPI) Stain (G1012, Servicebio) was applied to the slides to create a circular region, followed by incubation for 10 min at room temperature under low-light conditions. The slides were placed in pH 7.4 PBS (cat# G0002, Servicebio) and washed three times for 5 min each by shaking in a pendulum

oscillator (SYC-Z100, Servicebio). After slight drying, the sections were sealed with an antifluorescence quenching sealing solution (G1401, Servicebio).

Immunohistochemistry was performed on 4-μm-thick placental sections obtained from pregnant women. Placental tissues from the various experimental groups were deparaffinized and rehydrated with graded ethanol solutions and distilled water. The slides were immersed in 0.01 mol/L sodium citrate buffer (pH 6.0) and heated in a 95 °C water bath for 30 min. Endogenous peroxidase activity was inhibited by treating the sections with 3% hydrogen peroxide. The sections were blocked with 3% BSA (Solarbio, China) for 20 min and incubated overnight at 4 °C with an anti-CMIP antibody. The slides were washed three times with PBS before being incubated with biotinylated anti-rabbit IgG for 50 min at room temperature. Diaminobenzidine (DAB) was applied to visualize the staining. Finally, the nuclei were counterstained with hematoxylin for 3 min at room temperature. PBS was used in place of the primary antibody as a negative control.

Cell culture

The HTR-8/SVneo cell line is a normal human extravillous trophoblast cell line derived from first-trimester placenta. JEG-3 is a malignant choriocarcinoma cell line cloned from the Erwin-Turner tumor (Woods strain) by Kohler et al. [20]. Both cell lines were sourced from the ATCC. The cells were cultured in 1640 medium (31800, Solarbio) supplemented with 10% fetal bovine serum (G24-70500, Genial), penicillin (100 U/mL), and streptomycin (100 μg/mL) at 37 °C and 100% humidity in a 5% CO2 atmosphere. The cells in the logarithmic growth phase were digested with 0.25% trypsin (SC107-01, Seven). A single-cell suspension was prepared, and the cells were seeded into the appropriate plates. The cells in the hypoxia group (H group) were cultured in 1% oxygen for various durations (6, 12, 24, 48, 72, or 96 h) in a humidified hypoxia workstation (InvivO2 400). The cells in the control group were cultured in 20% oxygen. Protein and RNA were collected within 1 min after treatment completion.

Primary placental trophoblast cells were isolated from healthy pregnant individuals undergoing elective termination during early pregnancy (8-12 weeks of gestation). The human study was approved by the Human Research Ethics Board of the Third Affiliated Hospital of Zhengzhou University, and informed consent was obtained from all participants prior to enrollment. The ethics approval reference number was 2022-338-01. The placental chorionic tissue was removed from the operating room of the Third Affiliated Hospital of Zhengzhou University, and washed with sterile normal saline, and the 1 mm chorionic villi were scraped with a scalpel for further shear separation. The separated chorionic villi were aspirated into a centrifuge tube along with saline, and centrifugation was performed at 1000 rpm for 2 min. The supernatant was discarded, and trypsin was added in an amount equal to that of the villi. Digestion was carried out for 10 min, after which an equal amount of medium was added to terminate the digestion, and centrifugation was carried out at a low speed of 1000 rpm for 2 min. The supernatant was removed, and medium was added to resuspend it. The suspension was transferred to culture flasks precoated with matrix gel for incubation. The state of the cells was observed after 3days, after which they were passaged according to the number of cells.

The slides containing primary extrachorionic trophoblast cells were fixed with 4% paraformaldehyde (2 ml) for 15 min, followed by the addition of 1xPBS (1 ml) and three washes, each lasting 3 min. The cells were permeabilized with 2 ml of 0.5% Triton X-100 (1xPBS) at room temperature for 15 min, followed by three washes with 1xPBS (1 ml) for 3 min on each slide. 5% goat serum (2 mL) was added, and the mixture was incubated at room temperature for 1 h. Then, the slides were washed three times by dipping them in 1 ml of 1xPBS for 3 min each. Next, 300 μL of diluted primary antibody (HLA-G: 1:200) was added to the dish and incubated at 4 °C overnight. A 1 ml dipwash with 1xPBS was performed three times for 3 min each. A diluted fluorescent secondary antibody (488, 1:1000) was added, and the mixture was incubated at room temperature for 1 h. The mixture was washed three times with 1 ml of 1xPBS for 3 min each. Note: Starting from the addition of the fluorescent secondary antibody, all subsequent steps were performed under dark conditions to minimize light exposure. The remaining nuclei were stained as follows: the samples were incubated with diluted DAPI (1:10) for 10 min, during which the nuclei were stained, and images were observed and collected under a fluorescence microscope.

Cell transfection

Small interfering RNAs (siRNAs) were obtained from GenePharma (China). The cells were divided into two groups: the SI-CMIP group which were transfected with siRNA targeting CMIP (siRNA-CMIP) in HTR-8/SVneo cells and the negative control group (SI-NC group) which were transfected with scrambled non-targeting siRNA sequence as negative control for siRNA-mediated knockdown experiments. Transfection was performed at a confluence of approximately 60% (approximately 14 h after seeding), and 5μL of each siRNA was transfected into the cells via 5μL of Lipofectamine RNAi MAX (13778-150, Thermo Fisher). Plasmids encoding Flag-CMIP (NM_198390.3, pcDNA3.1) and His-PDE7B (NM 018945.4, pcDNA3.1)

were synthesized and purchased from GeneCreate (Wuhan, China). These two plasmids were transfected into HTR-8/SVneo cells for an immunoprecipitation experiment, in which Flag-CMIP was the bait protein and His-PDE7B was the prey protein. For plasmid transfection, a plasmid overexpressing PDE7B (NCBI gene ID: 27115, pIRES2-DsRed2) from the Public Protein/Plasmid Library (PPL, Nanjing, China) was used. The cells were divided into two groups: the OE-CMIP+PDE7B group (CMIP-overexpressing cells subsequently transfected with PDE7B expression plasmid) and the OE-CMIP+NC group (control group for plasmid transfection, CMIP-overexpressing cells transfected with empty vector). Transfection was performed at a confluence of approximately 60% (approximately 14 h after seeding), and 2.5 μg of plasmid was transfected into the cells via 5μL of Lipofectamine 3000 (L3000015, Thermo Fisher). After 48 h of transfection, the cells were collected for quantitative reverse transcription PCR (qRT-PCR) or Western blot analysis to determine the transfection efficiency. The siRNA sequences are shown in Table S2. Transfection was performed according to the manufacturer's protocols (Invitrogen; Thermo Fisher Scientific). All transfections were performed transiently.

Lentivirus infection

A lentivirus overexpressing CMIP was obtained from GeneChem (Shanghai, China). The cells were divided into two groups: the OE-NC group (negative control for overexpression experiments, transduced with empty lentiviral vector) and the OE-CMIP group (HTR-8/SVneo cells transduced with lentivirus overexpressing the CMIP gene). Preliminary tests revealed that the ideal multiplicity of infection (MOI) for the lentivirus was 40. When HTR-8/SVneo cells reached 20-30% confluence, they were transduced with the lentivirus using HitransG lentivirus infection reagent (GeneChem) for 48 h, following the manufacturer's instructions. Two days after transduction, the cells were screened with 2 μg/mL puromycin (Beyotime Biotechnology) for one week to establish stably transduced cell lines. The overexpression of CMIP was confirmed by Western blotting and qRT-PCR.

qRT-PCR

Total cellular RNA was extracted via TRIzol reagent (cw0580s, CWBIO), and reverse transcription was performed via ReverTra Ace qPCR RT Master Mix (FSQ-201, TOYOBO). Less than 1 μg of mRNA was reverse transcribed into cDNA with a GeneAmp® PCR System 9700 (805S4151578, Thermo Fisher Scientific). Relative mRNA levels were determined via the use of an Ultra SYBR mixture (AQ601-01-V2; Transgene Biotech) for polymerase chain reaction amplification. Quantitative PCR (qPCR) was performed on a CFX96 instrument (794BR12474, Bio-Rad). All measurements were normalized against endogenous GAPDH and calculated as relative expression levels compared with those of their untreated counterparts via the $2^{-\Delta\Delta Ct}$ method. Three biological replicates of HTR-8/SVneo cells were included. Table S1 lists the sequences of the primers.

Western blot analysis

The cells were lysed in ice-cold cell lysis buffer (PC101, Yazyme) and RIPA lysis buffer (LT101, Yazyme), each containing a protease/phosphatase inhibitor cocktail (Servicebio, G2007-1ML). The protein concentrations were measured with a BCA protein assay kit (SW201-02, SEVEN). An Omni-EasyTM one-step PAGE Gel Rapid Preparation Kit (PG211, Yazyme) was used to prepare electrophoretic gels for Western blotting. The protein samples were separated by electrophoresis, transferred to 0.45-μm PVDF (IPVH00010, Millipore) membranes, and incubated overnight at 4 °C with primary antibodies. Details of the antibodies used are shown in the major resources table. The membranes were incubated for one hour at room temperature with either a goat anti-rabbit/mouse IgG fluorescent secondary antibody or an HRP-conjugated secondary antibody. The gel was visualized with an imaging system, the images were processed, and the gray values of the protein bands were evaluated via ImageJ software (2.14.0). The relative expression of each target protein was determined via the use of GAPDH as the endogenous control gene. Three biological replicates of HTR-8/SVneo cells were used.

Cell viability, migration, invasion, and endothelial-like tube formation assays

A Cell Counting Kit-8 (CCK-8) (MA0218, Meilunbio) was used to measure changes in cell viability following transfection and infection. A longitudinal scratch was made in the cell layer in a six-well plate, and the wound was photographed under a microscope. ImageJ software was used to determine the wound area from the photographs. The wound healing percentage was calculated via the formula (A0 - A24/A48)/A0 × 100%, where A0, A24, and A48 represent the scratch areas at 0, 24, and 48 h, respectively. Matrigel (356,234, Corning) was diluted at a ratio of 1:8 and placed at the bottom of a chamber. After the upper chamber was hydrated, 200 μL of suspended cells in serum-free medium was added. In the lower chamber, 600 μL of 10% FBS medium was added. The cells were fixed with 4% paraformaldehyde and stained with crystal violet, and four fields

per chamber were photographed to calculate the mean cell number. Three biological replicates of HTR-8/SVneo cells were used. For the endothelial-like tube formation assay, growth factor-reduced Matrigel (082704, ABW) was frozen on ice overnight and diluted 1:1 (vol/vol) with 1640 medium containing 0.1% FBS. Then, 50μL of the diluted Matrigel was added to each well of a 96-well plate and incubated at 37 °C for two hours to allow solidification. HTR-8/SVneo cells were transfected for 24 h. A total of 3 × 10^4 cells suspended in 50μL of 1640 medium supplemented with 0.1% FBS were plated in each well and incubated at 37 °C for eight hours. Digital images were captured via an Olympus IX71 inverted microscope, and the number of junctions was determined via ImageJ software (2.14.0).

Transcriptome sequencing

Three biological replicates of HTR-8/SVneo cells were used for both the CMIP-knockdown (SI-NC, SI-CMIP) and CMIP-overexpressing (OENC, OE-CMIP) groups. To analyze gene expression profiles, RNA from twelve cell lines was sequenced by Shanghai Meiji Biomedical Technology Co., Ltd. mRNA was isolated from total RNA via magnetic beads bound to oligo dT, facilitating A-T base pairing and poly-A selection. The isolated mRNA was then subjected to fragmentation via fragmentation buffer, generating fragments of approximately 300 bp. cDNA was synthesized from the fragmented mRNA via reverse transcriptase. Adaptors were ligated to the cDNA, and the resulting libraries were sequenced on an Illumina platform. The sequencing data were analyzed online via the Major BioCloud Platform (https://www.majorbio.com). Genes with a|log2FC| ≥ 1.00 and a p value < 0.05 were considered significantly differentially expressed.

Co-IP (coimmunoprecipitation)

Lysis buffer was added to a cell culture plate to lyse the cells at 4 °C. The lysate was centrifuged at 12,000 rpm for 10 min, and the supernatant was collected for further analysis. A small aliquot of lysate was collected and used in subsequent experiments. The remaining lysate was incubated overnight at 4 °C with 10 μg of rabbit anti-Flag antibody (3064, DIA. AN) or control IgG from the same species. PierceTM protein A/G agarose beads (Thermo et al.) were thoroughly washed with lysis buffer. The pretreated beads were mixed with the cell lysate, incubated overnight at 4 °C, and then centrifuged at 2500 rpm for 3 min at 4 °C. The supernatant was discarded, and the agarose beads were rinsed three times with 1 ml of lysis buffer. After 100μL of 2xSDS loading buffer was added, the samples were incubated at 95 °C for 5 min before being analyzed by Western blotting. A list of the antibodies used in this study is presented in the major resources table (Supplementary Material 1).

Enzyme-linked immunosorbent assay (ELISA)

After incubation, HTR-8/SVneo cells (4 × 105) were harvested, and the protein concentrations were measured via a BCA protein assay kit (SW201-02, SEVEN). (1) For the dilution of standard protein, standard protein was diluted with PBS, and the initial concentration of standard protein was 0.5 mg/ml. The standard protein and PBS were added in appropriate proportions to seven EP tubes labeled A, B, C, D, E, F, and G at concentrations of 0, 0.05, 0.1, 0.15, 0.2, 0.3, and 0.4 mg/ml. (2) The sample was diluted 10-fold by adding 4.5μL of the sample to 40.5μL of PBS. (3) Preparation of the BCA working solution: The total volume of the BCA working solution was calculated according to the formula. The BCA working solution was prepared by mixing the BCA-A solution and B solution at 50:1, and the mixture was mixed well. (4) Quantitative detection: Each well of a 96-well plate was loaded with 20μL of standard protein or sample, followed by 200μL of BCA working solution. The plate was incubated at 37 °C for 30 min and cooled to room temperature; the absorbance values of the proteins were measured in the range of 540–590 nm via a microplate reader. The detection process was completed within 5 min. (5) Plotting the standard curve: The standard curve was generated by plotting the difference between the standard absorbance and blank absorbance on the x-axis and the corresponding protein concentration on the y-axis. The average concentration of each sample was calculated and incorporated into the plot. The cells were subsequently centrifuged at 12,000 xg for 15 min at 4 °C. The concentration of cyclic adenosine phosphate (cAMP) in the cell supernatant was quantified via an enzyme-linked immunosorbent assay (ELISA) kit (E-EL-0056, Elabscience) according to the manufacturer's protocol. The absorbance was measured at 450 nm via a microplate reader (model No. 1408072; Bio-Tek, USA).

Animal study

Sprague-Dawley rats aged 8-10 weeks and weighing 170–200 g were obtained from Zhengzhou University Experimental Animal Center. All animals were fed conventional laboratory food and housed on a 12:12-hour light/dark cycle. If a vaginal plug was detected, the day was considered gestational day (G)1. Preeclampsia (PE) was induced by the oral administration of N(ω)-nitro-L-arginine methyl ester (L-NAME, 300 mg/kg/day; N814751, Macklin) between GD6 and GD19. The experiments were approved by the Research Ethics Approval Committee of

the Laboratory Animal Center of Zhengzhou University (Approval No. ZZU-LAC20230210 [07]) and complied with the ARRIVE Guidelines and NIH regulations on the care and use of laboratory animals. Pregnant rats were randomly assigned to one of four groups: the control ($n=3$), L-NAME ($n=5$), L-NAME+AAV9-CON ($n=3$), and L-NAME+AAV9-CMIP ($n=5$) groups. Adeno-Associated Virus 9-CMIP(AAV9-CMIP) and Adeno-Associated Virus 9-CON(AAV9-CON) were acquired from GeneChem in Shanghai, China. A total of 2.5E+12 vg of adenovirus was injected into the tail vein at G1. Systolic blood pressure (SBP) was measured on G5, G10, G13, G16, and G19 via tail-cuff plethysmography (BP-2010 A, Softron). Before measurement, the rats were restrained and placed in the chamber at a constant temperature of 32 °C for 15-20 min to allow them to calm down, and then five consecutive measurements were taken at intervals of 1 min. The rats were allowed to rest for 5 min before the next measurement. All pregnant rats were euthanized under isoflurane anesthesia (Ruiwode Life Science, Shenzhen, China) on GD20, and the placental fetuses were collected for further analysis. Placentas were collected on G20 for histological analysis, weight measurement, and CMIP protein level analysis via immunofluorescence. The weights of the maternal and fetal rats were also measured on the indicated days.

Statistical analysis

SPSS (Version 27.0, IBM, New York, USA) and GraphPad Prism (Version 9, Inc., San Diego, CA, USA) were used for statistical analysis. The Shapiro-Wilk test was used to assess the normality distribution of the data. Student's t test or the Mann-Whitney test was performed to compare data between two groups. Welch's ANOVA and Welch's t tests were used to correct for variance when it was inconsistent. The data are expressed as the means ± SEMs. A P value of <0.05 was considered to indicate statistical significance. The representative images were chosen from one of the repeats that best matched the average data in each experiment. (*$P<0.05$, **$P<0.01$, ***$P<0.001$, ****$P<0.0001$; NS, not significant).

Results

CMIP expression decreased in chorionic extravillous trophoblasts in PE

We first examined CMIP expression patterns and localization in placental tissues from women with preeclampsia and normotensive controls to explore its potential role in PE pathogenesis. Multiplex immunofluorescence revealed that CMIP colocalized with HLA-G, a specific marker of extravillous trophoblasts (EVTs), in the cytoplasm and cytomembrane of EVTs (Fig. 1A), and immunohistochemistry confirmed that CMIP was expressed in both EVTs and syncytiotrophoblasts (STBs) (Fig. 1B). To further validate these findings, immunofluorescence staining was conducted on an additional 40 randomly selected fresh placental tissues (20 PE vs. 20 NP). This analysis revealed significantly lower CMIP expression levels in the EVTs of PE patients compared to NP controls (Fig. 1C). Furthermore, immunohistochemical analysis of 16 randomly selected samples (8 PE vs. 8 NP) demonstrated reduced CMIP expression in both EVTs and STBs in PE placentas (Fig. 1D and E). Both methodologies consistently indicated decreased CMIP expression in PE placental tissues, particularly within EVTs, suggesting its potential role in PE pathogenesis.

CMIP enhances the invasion, migration, proliferation and tube-formation ability of EVTs

To investigate whether CMIP contributes to the pathogenesis of PE by regulating trophoblast function, we examined the effects of its overexpression or knockdown on trophoblast cells. Notably, CMIP knockdown reduced the proliferative (Fig. 2A), migratory (Fig. 2C), invasive (Fig. 2E), and angiogenic capacity (Fig. 2F) of HTR-8/SVneo cells. Conversely, when CMIP expression levels were increased, the proliferative capacity of HTR-8/SVneo cells remained unchanged (Fig. 2B), whereas their migratory (Fig. 2C), invasive (Fig. 2E), and angiogenic capacity increased (Fig. 2F).

CMIP promotes the function of EVTs through the PDE7B-cAMP pathway

To investigate the molecular mechanisms underlying the impact of CMIP expression on trophoblast function, we performed RNA sequencing on HTR-8/SVneo cells with CMIP knockdown or overexpression, as well as their respective control cells. The results revealed that CMIP overexpression (Fig. 3A) led to increases in the expression of 63 genes and decreases in the expression of 37 genes. However, after CMIP knockdown (Fig. 3B), the expression of 103 genes increased, whereas that of 85 genes decreased. The enrichment analysis of sequencing data suggested that CMIP may regulate trophoblast function through distinct signaling pathways depending on its expression levels. In CMIP-overexpressing HTR-8/SVneo cells, transcriptomic and functional data were associated with tissue morphogenesis, the NF-κB/TNF signaling pathway, hypoxia-related transcription, and cardiac development (Fig.S3). Conversely, CMIP-knockdown models showed activation of

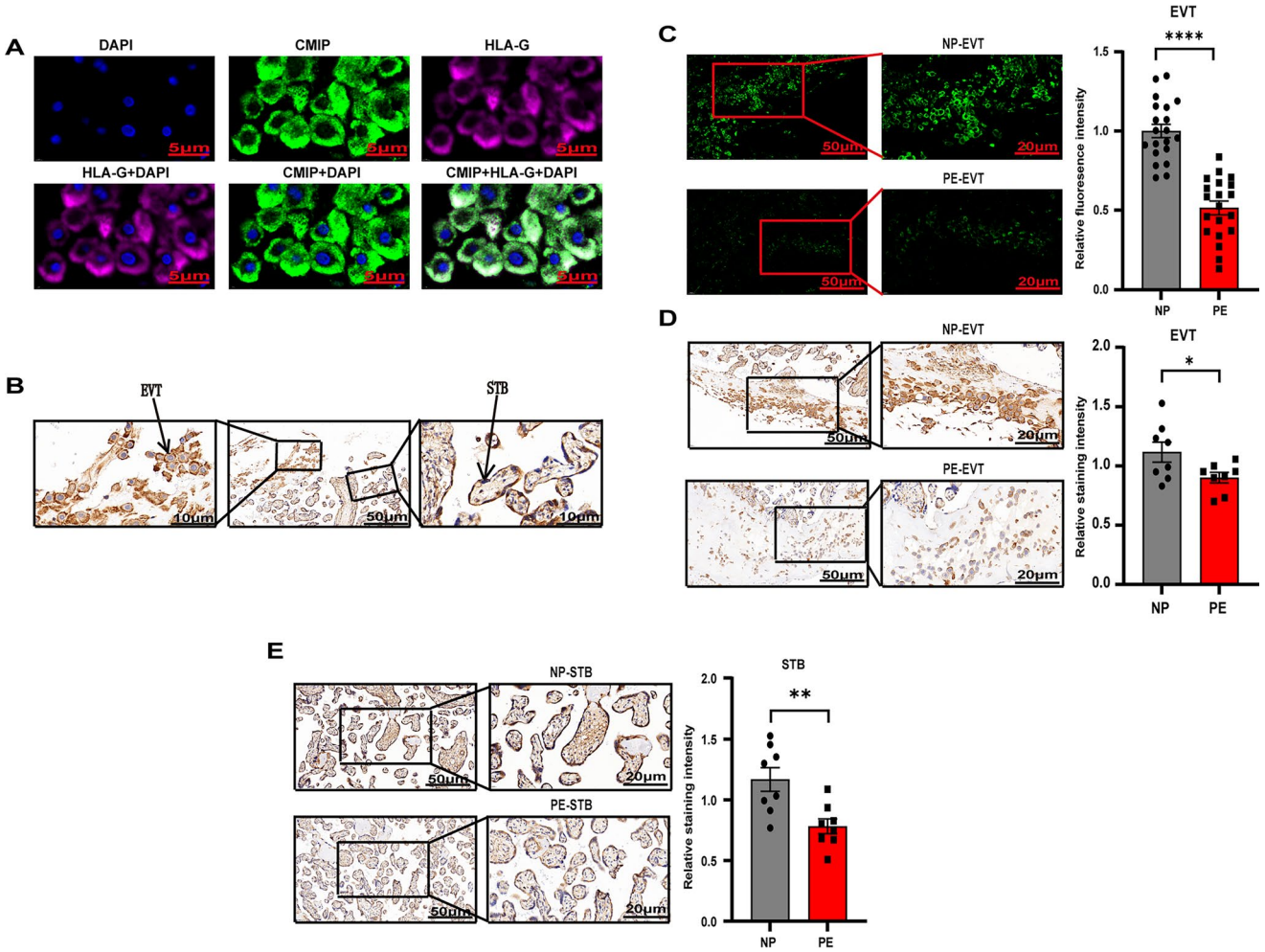

Fig. 1 CMIP localization and expression patterns in placental tissues from the normal pregnancy (NP) and preeclampsia (PE) groups. **A** Triple immunofluorescence staining of the human placenta showing that CMIP (green) colocalized with HLA-G (EVT marker, purple) and DAPI (nuclei, blue). Scale bar: 5 μm. **B** Immunohistochemical (IHC) localization of CMIP in STBs and EVTs (black arrows). Scale bars: 50 μm (overview) and 10 μm (inset). Representative images from the NP group. **C** Quantitative analysis of CMIP fluorescence intensity in EVTs (NP: $n=20$; PE: $n=20$). Scale bars: 50 μm (overview) and 20 μm (inset). **D**-**E** IHC-based semiquantitative analysis of CMIP expression in EVTs and STBs (NP: $n=8$; PE: $n=8$). Scale bars: 50 μm (overview) and 20 μm (inset). The data represent the means ± SEM. For all panels, the staining intensity was quantified by averaging ≥ 20 cells per section and was normalized to the control group mean. Student's t-test: $^{*}P<0.05$, $^{**}P<0.01$, $^{****}P<0.0001$. EVT: extravillous trophoblast; STB: syncytiotrophoblast

IL-17 signaling and dysregulated oxidative phosphorylation pathways, potentially reflecting the inflammatory stress and mitochondrial dysfunction characteristic of preeclampsia (Fig.S4). Joint analysis revealed that enriched GO terms were potentially associated with cAMP signaling (Fig.S5).

Joint screening was employed to identify factors exhibiting significant variations in expression following CMIP overexpression and knockdown. qRT-PCR was subsequently utilized to validate the alterations in the RNA expression of these factors. Notably, an increase in CMIP expression led to a decrease SMOC1 and PDE7B expression, whereas a decrease in CMIP expression resulted in increased SMOC1 and PDE7B expression (Fig. 3C). These findings were consistent with the sequencing data. Further experiments were conducted to validate changes in protein expression levels, revealing that PDE7B protein expression was low when the CMIP protein level was high; conversely, PDE7B expression was high when the CMIP protein level was low (Fig. 3D). However, no significant change in SMOC1 protein expression was detected (Fig. S1C). To further explore potential protein–protein interactions, we subsequently conducted immunoprecipitation (Co-IP) assays. The Co-IP results confirmed that CMIP physically interacts with PDE7B, providing further evidence of their functional association (see Fig. 3E). When CMIP was knocked down in HTR8 cells, RNA sequencing revealed the upregulation of PDE3A, which is involved primarily in the cGMP pathway [21]. However, neither the knockdown nor the

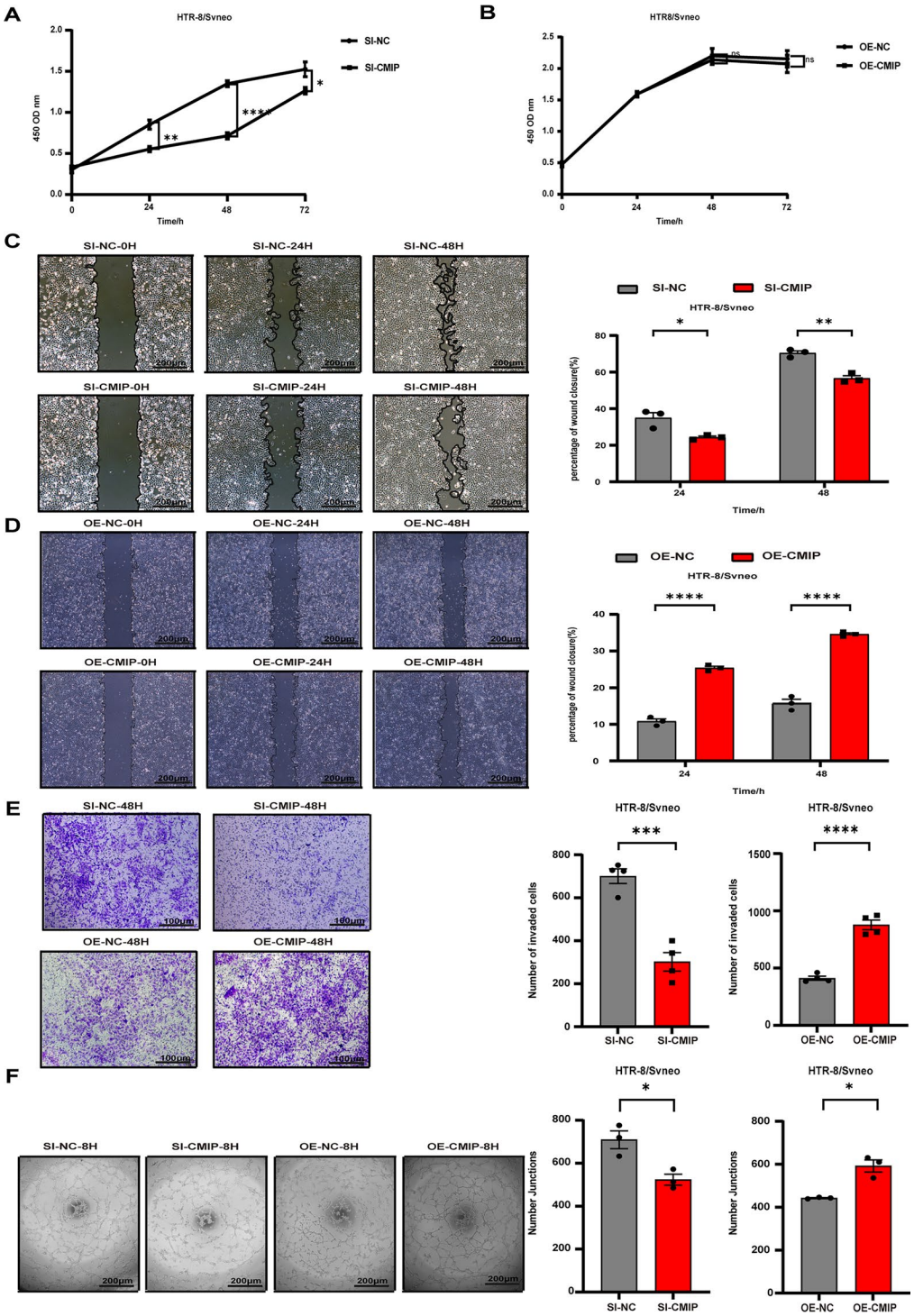

Fig. 2 CMIP overexpression enhances the proliferation, migration, invasion, and tube formation of HTR-8/SVneo trophoblasts. **A**-**B** Cell viability was assessed by a CCK-8 assay in the CMIP-knockdown (SI-CMIP vs. SI-NC) and CMIP-overexpressing (OE-CMIP vs. OENC) groups at the indicated time points ($n=3$). **C**-**D** Representative images (0/24/48 h post scratching; scale bar: 200 μm) and quantitative analysis of the results of the wound healing assay ($n=3$). **E** Transwell invasion assay images (scale bar: 100 μm) and quantification of invaded cells ($n=4$). **F** Tube formation assay (scale bar: 200 μm) with branch point quantification ($n=3$). Data: mean ± SEM; Student's t-test; $^{*}P<0.05$, $^{**}P<0.01$, $^{***}P<0.001$, $^{****}P<0.0001$; NS: nonsignificant ($P>0.05$). SI-NC: negative control for knockdown; SI-CMIP: CMIP-knockdown; OE-NC: negative control for overexpression; OE-CMIP: CMIP-overexpression

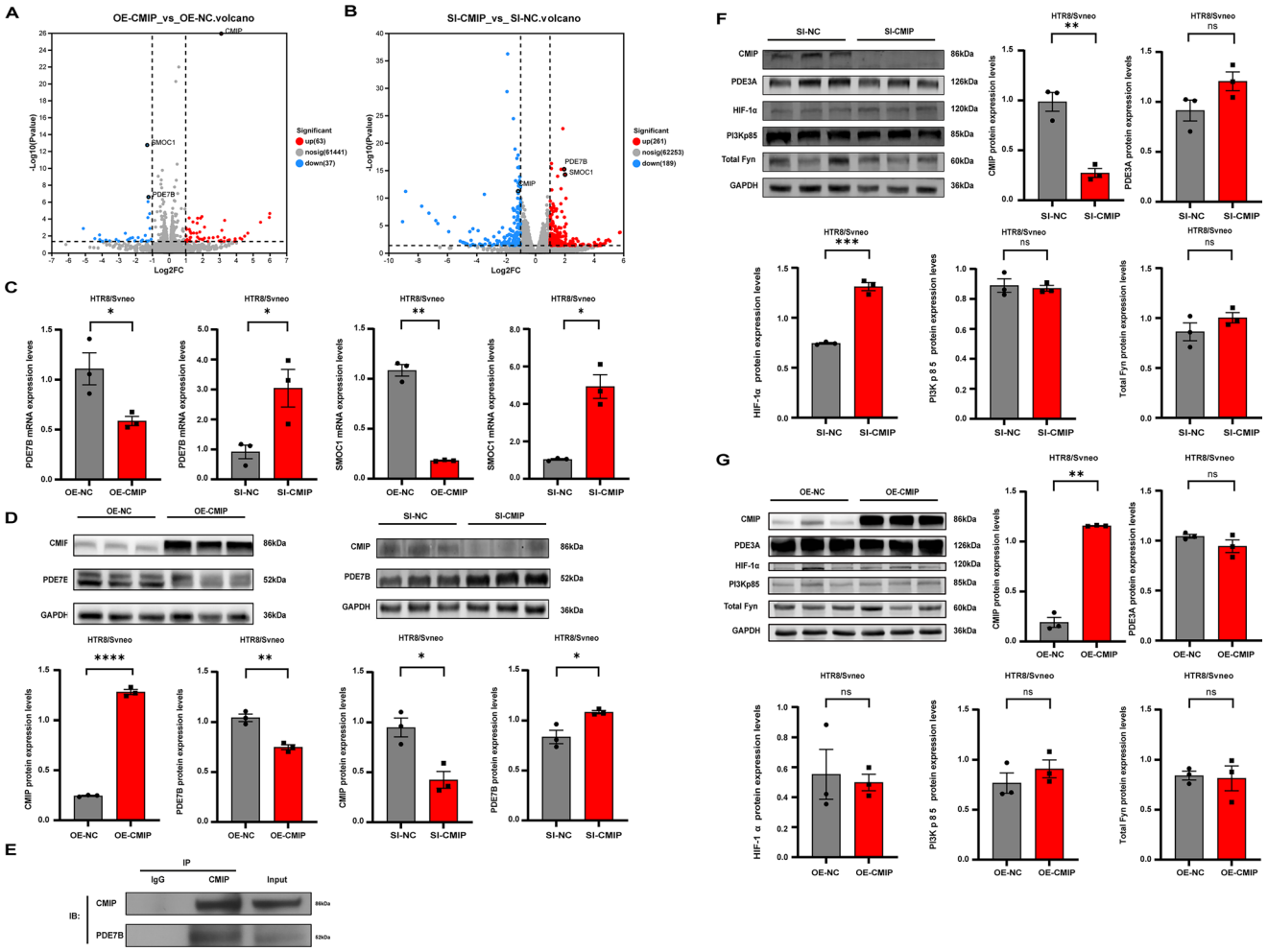

Fig. 3 Analysis and validation of RNA sequencing data from HTR-8/SVneo cells. **A**-**B** Volcano plots depict differentially expressed genes (DEGs) between the CMIP-overexpressing groups (OE-NC vs. OE-CMIP) and the CMIP-knockdown groups (SI-NC vs. SI-CMIP), filtered by|log2FC| ≥1.00 and $P<0.05$ ($n=3$). **C** qRT–PCR validation of PDE7B and SMOC1 mRNA levels in the CMIP-overexpressing (OE-CMIP) and CMIP-knockdown (SI-CMIP) groups versus the control group ($n=3$). **D** Western blot (WB) quantification of CMIP and PDE7B protein levels in the overexpression and knockdown groups ($n=3$). **E** Coimmunoprecipitation (Co-IP) assay showing the interaction of CMIP-PDE7B with HTR-8/Svneo cell lysates using a CMIP antibody for IP, followed by immunoblotting (IB) with anti-CMIP and anti-PDE7B antibodies. **F**-**G** WB analysis of CMIP, Total Fyn, PI3Kp85, HIF-1α, and PDE3A protein expression in CMIP-modulated cells (OE-CMIP and SI-CMIP) and their quantitative densitometry ($n=3$). The data are presented as the means±SEMs. Statistical significance was determined by two-tailed Student's t test: $^{*}P<0.05$, $^{**}P<0.01$, $^{***}P<0.001$, $^{****}P<0.0001$; NS: not significant

overexpression of CMIP altered PDE3A protein levels, indicating that CMIP does not regulate the cGMP pathway through PDE3A (Fig. 3F and G). Furthermore, Western blot analysis revealed no significant changes in the expression of PI3K or Fyn-proteins previously linked to CMIP in nontrophoblastic cells-following CMIP knockdown or overexpression (Fig. 3F and G). The data above demonstrate a strong association between PDE7B expression and CMIP levels.

We further investigated the interaction between PDE7B and CMIP in placental tissue. Multiplex immunofluorescence staining revealed that PDE7B, CMIP, and HLA-G were colocalized (Fig. 4A). PDE7B and CMIP colocalized in EVTs and were both found in the cytoplasm and cytomembrane. These findings indicate that PDE7B interacts with CMIP in the cytoplasm and cytosol of EVTs. To further elucidate the functional implications, a plasmid overexpressing PDE7B was transfected into HTR8/SVneo cells that had been stably transfected with CMIP (Fig. 4B). The experimental findings indicated that PDE7B overexpression attenuated the proliferation (Fig. 4C), invasion (Fig. 4D), migration (Fig. 4E), and angiogenic capacity (Fig. 4F) of trophoblasts. These findings suggest that the reduced expression of CMIP observed in PE patients may impair EVT function by modulating PDE7B activity.

PDE7B has been demonstrated to specifically hydrolyze cAMP [22, 23].As a critical regulatory enzyme, PDE7B maintains intracellular cAMP homeostasis through hydrolysis of this second messenger, consequently controlling

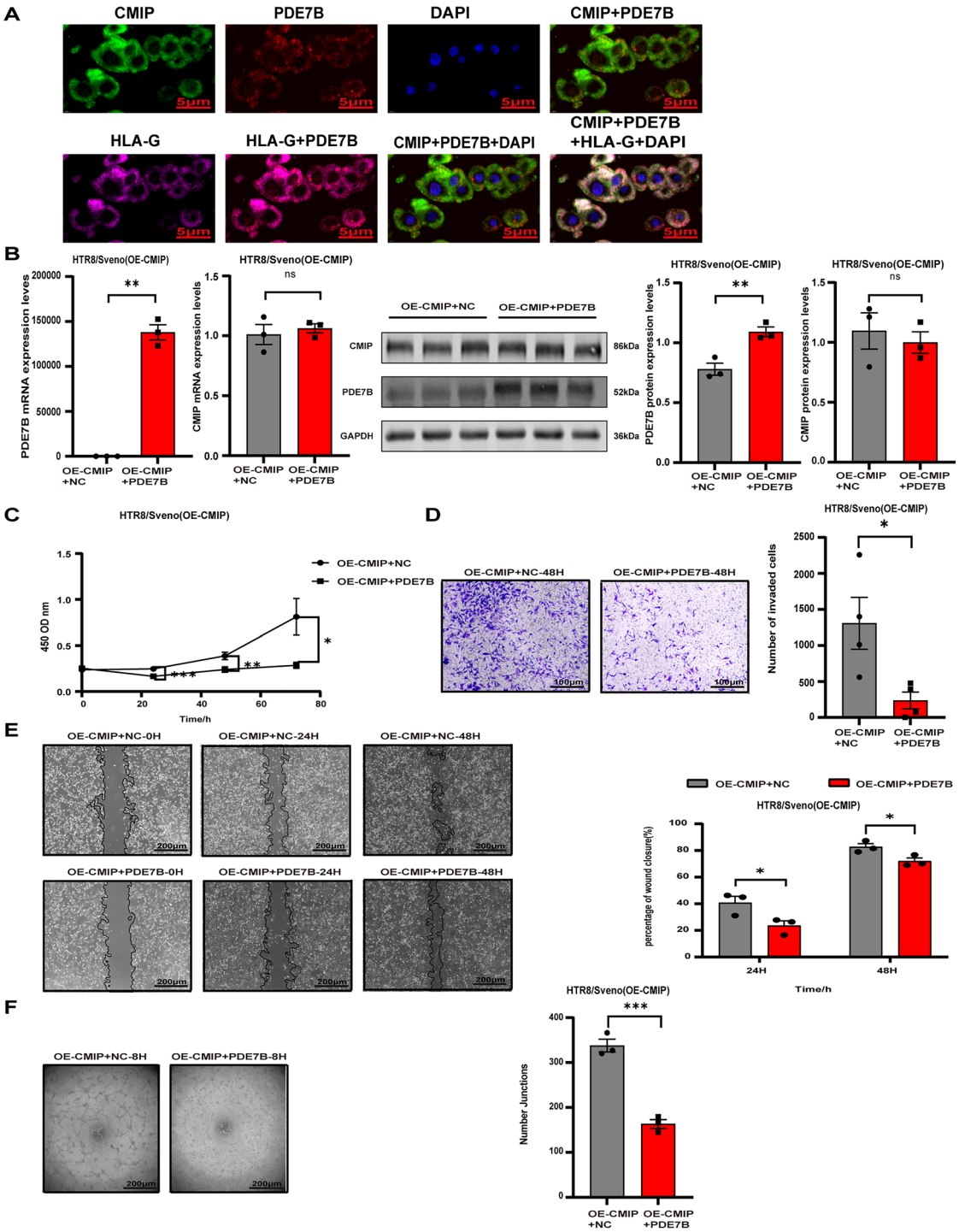

Fig. 4 Overexpression of PDE7B reverses CMIP-induced functional enhancement in HTR-8/SVneo cells. **A** Quadruple immunofluorescence staining of human placental tissues showing colocalization of CMIP (green), HLA-G (purple, indicating extravillous trophoblasts), PDE7B (red), and DAPI (nuclei, blue). Scale bar: 5 μm. **B** PDE7B and CMIP expression levels in HTR-8/SVneo cells were analyzed by qRT-PCR and Western blotting. OE-CMIP: cells with overexpressing CMIP; OE-CMIP+NC: OE-CMIP cells transfected with empty vector; OE-CMIP+PDE7B: OE-CMIP cells transfected with PDE7B plasmid. **C**–**F** Functional assays in OE-CMIP cells after PDE7B overexpression: **C** Cell viability (CCK-8 assay, $n=3$); **D** Transwell invasion assay ($n=4$; scale bar: 100 μm); **E** Wound healing migration ($n=3$; scale bar: 200 μm); **F** Tube formation assay ($n=3$; scale bar: 200 μm). The data are presented as the means ± SEMs. Statistical significance was determined by Student's t test; $^{*}P<0.05$, $^{**}P<0.01$, $^{***}P<0.001$, $^{****}P<0.0001$; NS: not significant

the activation status of downstream effectors including protein kinase A (PKA). cAMP serves as a universal secondary messenger essential for intracellular signal transduction. Collectively, the PDE7B-cAMP axis constitutes a pivotal control node governing the spatiotemporal dynamics of cAMP-mediated signaling. By evaluating the impact of changes in the CMIP expression level on cAMP concentrations and the expression of its downstream factor PKA, we aimed to determine whether CMIP modulates PDE7B-associated signaling pathways. ELISAs revealed that CMIP overexpression significantly increased cAMP levels (Fig. 5A) in the supernatant of HTR8/SVneo cells,

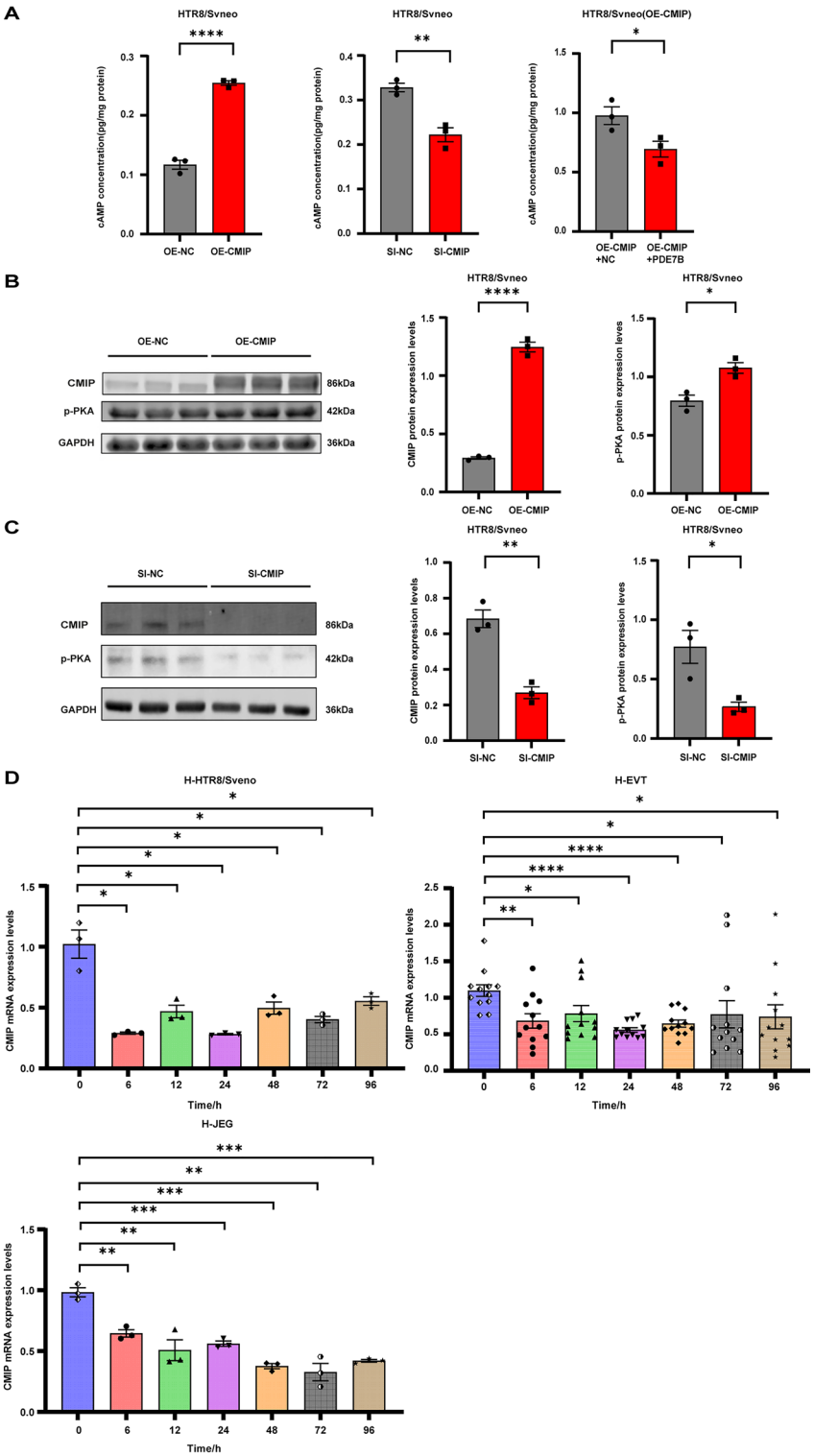

Fig. 5 CMIP regulates cAMP/PKA signaling via PDE7B and is downregulated under hypoxia in trophoblasts. **A** cAMP levels in HTR-8/SVneo cells measured by ELISA: CMIP overexpression (OE-CMIP vs. OE-NC), knockdown (SI-CMIP vs. SI-NC), and PDE7B overexpression (OE-CMIP + PDE7B vs. OE-CMIP + NC) groups ($n = 3$). **B**-**C** Western blot and quantification of CMIP and p-PKA protein levels in CMIP-overexpressing (OE) and CMIP-knockdown (KD) cells normalized to the level of GAPDH ($n = 3$). **D** qRT–PCR analysis of CMIP mRNA expression in HTR-8/SVneo ($n = 3$), primary extravillous trophoblasts (EVTs, $n = 12$), and JEG-3 cells ($n = 3$) under hypoxia (0–96 h). H- denotes the hypoxia-treated groups. H-HTR-8/SVneo cells/JEG-3 cells/EVT indicates HTR-8/SVneo cells, JEG-3 cells, and EVTs after hypoxia. EVT indicates primary extravillous trophoblast. Data: mean ± SEM; Student's t-test; $^{*}P < 0.05$, $^{**}P < 0.01$, $^{***}P < 0.001$, $^{****}P < 0.0001$

whereas CMIP knockdown resulted in a decrease in cAMP levels (Fig. 5A). Notably, the cAMP level was lower in the PDE7B-overexpressing (OE-CMIP+PDE7B) group than in the control group (Fig. 5A). Protein kinase A (PKA) serves as a key downstream effector of the cAMP signaling pathway. Western blot analysis revealed that CMIP overexpression increased PKA levels (Fig. 5B), whereas CMIP knockdown decreased PKA levels (Fig. 5C). These findings suggest that CMIP directly interacts with PDE7B to regulate the cAMP/PKA pathway, thereby influencing trophoblast function and contributing to the pathogenesis of PE.

Hypoxia reduces CMIP levels in trophoblasts

Among the recognized pathogeneses of PE, placental hypoxia due to impaired trophoblast remodeling is an important mechanism that triggers preeclampsia [2]. To investigate the cause of decreased CMIP levels in trophoblasts, we cultured three types of trophoblasts-primary cultures, HTR-8/SVneo cells, and JEG-3 cells-under hypoxic conditions. qRT–PCR analysis (Fig. 5D) revealed that, compared with those at 0 h, the CMIP RNA levels were lower in all three cell types after 6, 12, 24, 48, 72, and 96 h of hypoxia. This alteration in CMIP levels was consistent with changes observed in clinical samples from PE patients, suggesting that placental hypoxia in preeclampsia may affect trophoblast function by modulating CMIP expression.

CMIP overexpression attenuates the phenotype of the preeclamptic rat model

Previous experimental findings suggest that reduced CMIP impacts EVT cellular function and is correlated with defective placental remodeling. To further clarify the role of CMIP in placental function, we investigated its effects in an L-NAME-induced PE rat model. The adenoviral vector AAV9-CMIP, designed to overexpress CMIP, was injected into PE model rats to determine whether CMIP overexpression affects the development of PE. Compared with the control group, the L-NAME group presented higher systolic blood pressure (SBP) values (Fig. 6A) and lower fetal and placental sizes and weights (Fig. 6B), confirming the successful establishment of the PE rat model. However, L-NAME-AAV-CMIP treatment significantly alleviated blood pressure (Fig. 6A) and increased fetal and placental number and weight (Fig. 6B) compared with those of the L-NAME-AAV-CON group. To investigate the role of CMIP in placental villous trophoblast cells in preeclampsia (PE) rats, we used HLA-G labeling to locate placental villous trophoblast cells. Compared with that in the control group, the area of HLA-G-labeled trophoblast cells in the L-NAME group was significantly reduced whereas the area of HLA-G-positive trophoblast cells in the L-NAME-AAV-CMIP group was increased compared with that in the L-NAME-AAV-CON group (Fig. 6C). Using multiplex immunofluorescence experiments, we further demonstrate that both CMIP and PDE7B are expressed in HLA-G-positive placental extravillous trophoblasts (Fig. 6D).

In addition, compared with that in the control group, the expression of CMIP was significantly decreased in the L-NAME group, whereas the expression level of PDE7B was significantly increased (Fig. 6E). In the L-NAME-AAV-CMIP group, the expression of CMIP was significantly greater than that in the L-NAME-AAV-CON group, whereas the expression of PDE7B was significantly lower (Fig. 6E). Taken together, these results suggest that the overexpression of CMIP may alleviate L-name-induced preeclampsia symptoms by affecting the function of trophoblast cells.

Discussion

It is widely acknowledged that PE is associated with impaired trophoblast function [24]. Identifying the biological factors that mediate abnormal trophoblast invasion and migration and the failure of spiral artery remodeling, as well as therapeutic targets for PE, is becoming a hot topic of research [25]. However, the pathophysiology of PE remains unclear [26]. In this study, we employed a combination of multiplex immunohistochemistry, transcriptomics, immunoprecipitation, and cell- and animal-based studies to investigate the role of CMIP in the pathogenesis of PE. Our findings suggest that hypoxia-induced reductions in CMIP expression and its regulation of the cAMP/PKA signaling pathway through PDE7B may be involved in the development of PE. Furthermore, our observations indicate that upregulating CMIP might alleviate symptoms associated with PE.

CMIP, an adaptor protein, has been implicated in various diseases, such as cancer, leukemia, liver disease, and nephropathy [11, 13, 16–18, 27]. In this study, we investigated the role of CMIP in the placental tissues of individuals with PE. The immunohistochemistry findings and immunofluorescence revealed a substantial decrease in the expression level of CMIP in the placentas of PE patients compared with those of healthy controls. Additionally, two pathologists used immunohistochemistry to assess CMIP expression levels in EVTs and STBs in a double-blinded manner, and the findings were consistent with our immunohistochemistry results. These findings provide valuable insights into the pathogenesis of trophoblast dysregulation in PE and suggest that targeting CMIP may hold promise as a therapeutic approach for PE.

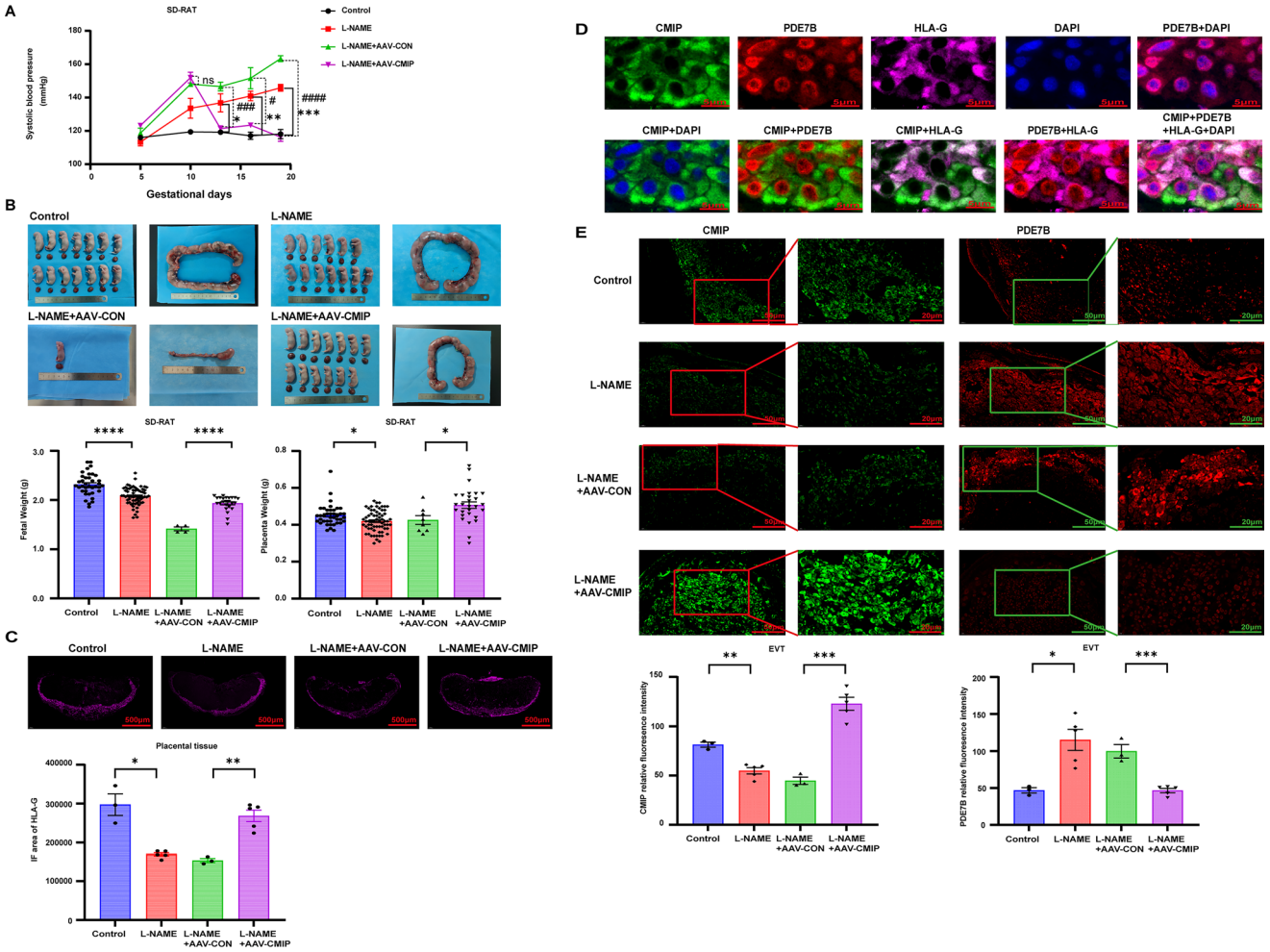

Fig. 6 Supplementation with adenoviral CMIP alleviates PE-related phenotypes in the L-NAME-induced PE rat model. **A** Dynamic changes in systolic blood pressure (SBP) across experimental groups: Control (saline, $n = 3$), PE model (L-NAME, $n = 5$), L-NAME + AAV-CON ($n = 3$), and L-NAME + AAV-CMIP ($n = 5$). **B** Representative images of fetal and placental morphology (top) and quantitative analysis of fetal weight/placental weight (bottom). **C** Immunofluorescence staining of HLA-G in placental extravillous trophoblasts (EVTs) (scale bar: 500 μm) and statistical analysis of the HLA-G-positive area. **D** Quadruple fluorescence colocalization of CMIP (green), HLA-G (purple), PDE7B (red), and DAPI (blue) in EVTs (scale bar: 5 μm). **E** Quantification of CMIP and PDE7B fluorescence intensity in placental EVTs (scale bars: 50 μm and 20 μm). The data are expressed as the means ± SEMs. Statistical significance was determined by Student's t test or the Mann-Whitney test. $*P<0.05$, $**P<0.01$, $***P<0.001$, $****P<0.0001$; $\#P<0.05$, $\#\#\#P<0.001$, $\#\#\#\#P<0.0001$; NS: not significant

The function of CMIP in trophoblasts has not been investigated. Placental defects in PE are caused mainly by insufficient trophoblast invasion and that CMIP promotes cancer cell proliferation, invasion, and metastasis [17]. On the bases of this evidence, we propose that the downregulation of CMIP suppresses trophoblast invasion and contributes to the pathogenesis of PE. Our experimental results demonstrated that CMIP promotes trophoblast invasion, migration, and vasculogenic capacity, whereas its low expression significantly inhibits these cellular functions. Furthermore, in vivo administration of CMIP effectively alleviated hypertension symptoms in a PE rat model, confirming the proposed hypothesis. These new findings add to our understanding of the relationship between CMIP and trophoblasts. Trophoblasts play a critical role in mediating maternal arterial transformation, which is essential for successful pregnancy [28, 29]. Our study may offer the possibility of altering pregnancy outcomes in PE.

We used RNA sequencing to validate changes in the expression of various genes, identifying those involved in signaling pathways downstream of CMIP and in the regulation of placental trophoblasts in PE. PDE7B and SMOC1 were the only two factors among the top ten DEGs that exhibited strong expression following CMIP knockdown, while their expression levels were low after CMIP overexpression. Experimental validation revealed that the changes in the RNA expression of PDE7B and SMOC1 were consistent with the sequencing results, but at the protein level,

only PDE7B exhibited consistent changes. As a result, subsequent studies focused on the interaction between PDE7B and CMIP. Multiplex immunofluorescence analysis revealed that PDE7B colocalized with CMIP and HLA-G in EVTs in human placental tissue. Interestingly, when we modulated the expression of CMIP, there were no changes in the protein expression of Fyn [12], PI3K [30], or the protein encoded by the differentially expressed gene PDE3A, which was shown to interact with CMIP in sequencing studies [12]. However, we acknowledge that this analysis did not investigate the phosphorylation status (active vs. inactive forms) of Fyn, which is critical for its downstream signaling functions. Future studies using phospho-specific antibodies or activity assays will be needed to fully resolve whether CMIP indirectly modulates Fyn kinase activity in trophoblasts. These findings suggest that the role of CMIP in trophoblasts is unique. Rescue experiments demonstrated that invasion was weakened after overexpression of PDE7B in trophoblasts stably overexpressing CMIP, further suggesting that PDE7B may act as a downstream target of CMIP in trophoblasts. The factors that interact with various cell types differ, which explains the diverse roles of CMIP in different disorders.

PDE7B expression changes in trophoblast cells in response to CMIP, emphasizing the potential contribution of PDE7B to pathological processes. PDE7B belongs to the phosphodiesterase (PDE) family and hydrolyzes the second messenger cAMP. PDE7B has been shown to have higher affinity and stronger selectivity for cAMP than PDE7A does [22, 23]. Our sequencing results revealed that PDE10A and PDE4D were also overexpressed when CMIP was expressed at low levels and were among the top ten DEGs. As both of these proteins specifically hydrolyze cAMP [31], these results indicate that cAMP may be involved in CMIP-associated signal transduction pathways. Because low levels of cAMP are associated with various diseases, PDE inhibitors that limit cAMP hydrolysis have been extensively researched as new drugs. The PDE superfamily members PDE4, PDE7, and PDE8 hydrolyze cAMP. PDE4 inhibitors have been used clinically for many years; however, owing to the effects of PDE4 inhibitors on nontarget tissues, they have numerous adverse effects [31, 32]. Research indicates that PDE7 inhibitors have fewer adverse effects than PDE4 inhibitors do, which could be attributed to the fact that PDE7 acts only in particular cells [33]. PDE7B modulates the cAMP system, which regulates inflammatory responses, cell growth and proliferation, gene transcription, memory formation, and cognition [34]. PDE7 inhibitors have demonstrated promising potential for treating neurological disorders (such as Parkinson's disease) [35], inflammatory diseases, and cancers. However, in most structure-based screening studies, the crystal structure of the PDE7A isoform is used. The lack of a structure for PDE7B has hampered the development and use of PDE7B inhibitors [33]. In trophoblastic cells, our findings provide an alternative approach for therapeutic strategies in which CMIP is targeted to regulate cAMP levels instead of PDE7B targeted to cAMP. In pregnancy-related diseases, the cAMP pathway is essential for trophoblast differentiation and development. It is primarily involved in trophoblast fusion [36], proliferation, invasion, and migration [37] and promotes angiogenesis [38]. As a pleiotropic second messenger, the downstream factor of cAMP includes the cAMP-dependent protein kinase PKA [39], which phosphorylates several kinases and promotes tumor cell proliferation, invasion, and metastasis [40]. RNA sequencing (RNA-seq) analysis revealed that CMIP critically regulates the cAMP signaling pathway. Experimental validation revealed a positive correlation between CMIP expression dynamics and cAMP/PKA levels, suggesting that CMIP modulates trophoblast function through cAMP–PKA axis regulation, potentially through its interaction with PDE7B.

The direct interaction between CMIP and PDE7B may regulate its function through multiple mechanisms. First, CMIP could act as a scaffolding protein to spatially modulate PDE7B activity (analogous to AKAPs anchoring PDE4 [41]) or induce allosteric changes in its catalytic domain (similar to calmodulin-mediated activation of PDE1 [42]). Second, CMIP may stabilize PDE7B via chaperone-like activity (e.g., as seen with HSP90 in kinase stabilization [42]), potentially inhibiting ubiquitin–proteasome degradation [43]. Such regulation could hold physiological significance in tissues reliant on localized cAMP signaling, such as immune or neuronal systems [41]. However, the precise mechanisms—including binding site mapping, catalytic modulation, and downstream effects–require further validation through truncation mutagenesis, in vitro activity assays, and ubiquitination profiling [44]. This study establishes a foundational framework for CMIP-PDE7B functional crosstalk, and future work should explore its dynamic role in cAMP signaling networks and potential pathological relevance.

Although our coimmunoprecipitation assays might suggest a direct physical interaction between CMIP and PDE7B in transfected HTR8/SVneo cells (Fig. 3E), fundamental differences existed between the overexpression system in HTR8/SVneo cells and the placental tissue microenvironment. In transfected cells, artificially elevated protein concentrations can stabilize weak or transient interactions that evade detection under physiological expression levels [45]. Furthermore, endogenous CMIP-PDE7B binding in placental tissue may be spatially restricted to specific subcellular compartments (e.g., migratory fronts) or regulated by posttranslational modifications that are absent in vitro [46].

Technical challenges in Co-IP of scarce clinical samples–including protease susceptibility and antibody affinity limitations, are well documented in trophoblast studies [47]. To address this, we are developing CRISPR/Cas9-mediated endogenous tagging models combined with proximity ligation assays (PLAs), which enable single-molecule visualization of interactions in living trophoblasts. Nevertheless, the conserved functional synergy between the cytoskeletal role of CMIP and the cAMP hydrolysis activity of PDE7B (Fig. 5) strongly supports its pathophysiological importance in placental development.

Hypoxia is a crucial factor in various pregnancy-related diseases. While a certain level of hypoxia is normal during early pregnancy, prolonged exposure to hypoxia can lead to complications such as PE and fetal growth restriction (FGR) [48, 49]. Our previous study demonstrated that hypoxia reduces the migration and invasion of HTR-8/SVneo cells, which corresponds to the invasion phase of extravillous trophoblasts [50]. We observed that exposure of trophoblasts to hypoxia downregulates the expression of CMIP and increases the protein level of HIF-1α after CMIP knockdown. This finding is consistent with the decreased expression of CMIP observed in placental trophoblasts in PE. Hypoxia plays a significant role in trophoblast dysfunction in the PE placenta and may also explain the reduced expression of CMIP in PE.

The dual regulatory role of hypoxia in trophoblast invasion presents an intriguing paradox that warrants careful interpretation. While previous studies have established hypoxia as a promoter of extravillous trophoblast (EVT) invasion through HIF-1α-mediated pathways such as urokinase-type plasminogen activator receptor (uPAR) upregulation [51] and TET1-dependent epigenetic modifications [52], our findings reveal a complementary regulatory mechanism involving CMIP downregulation through the PDE7B-cAMP axis. This apparent contradiction may reflect the complex spatiotemporal regulation of placental development, where the severe hypoxia (1% O_2) employed in our model [50], in contrast with the milder hypoxia (3-5% O_2) typically associated with proinvasive effects, potentially activates compensatory mechanisms to prevent excessive tissue remodeling. The observed HIF-1α elevation under 1% O_2 coexists with CMIP suppression, suggesting a bifurcation in HIF-1α signaling: while canonical pathways increase invasion via matrix metalloproteinases (MMPs) and uPAR, parallel signaling through CMIP-PDE7B-cAMP may impose critical constraints on invasion dynamics. This dual regulation likely maintains equilibrium between physiological placentation and pathological overinvasion, with cell-type specificity (e.g., HTR-8/SVneo vs. primary EVTs) and oxygen gradient variations further modulating these responses. Our identification of CMIP as a hypoxia-responsive brake mechanism expands the current understanding of invasion regulation, potentially explaining how aberrant HIF-1α activation in pregnancy complications such as preeclampsia could disrupt this balance through disproportionate CMIP suppression. Future investigations exploring temporal oxygen fluctuations, interpathway crosstalk (particularly between cAMP signaling and the MMP/uPAR systems), and comparative analyses across trophoblast models will be essential to elucidate how these opposing signals integrate during normal and compromised pregnancies.

In RPL B cells [53], ER stress triggers PERK-ATF4-dependent RNF20 upregulation, promoting CMIP proteasomal degradation, while analogous TERT-mediated mechanisms were observed in allergic rhinitis DCs [54]. Hypoxia, a known ER stress inducer [55], likely drives similar ubiquitination pathways in PE. While the stable CMIP mRNA levels in RPL B cells support the predominance of post-translational regulatory mechanisms, transcriptional regulation of CMIP by hypoxia remains plausible. Future studies should delve into hypoxia-specific mechanisms, including potential cross-regulatory networks between HIF-1α and ER stress, to fully elucidate the molecular mechanisms underlying CMIP downregulation in PE.

To gain further insights into the role of CMIP in PE, we used L-NAME to establish a PE rat model. L-NAME limits endothelial nitric oxide synthase (eNOS)-mediated NO generation and thereby prevents vasodilation, resulting in increased arterial blood pressure [56]. Our findings demonstrated that a CMIP-overexpressing adenoviral-mediated reduction in blood pressure attenuated placental underdevelopment and increased fetal survival, suggesting that this intervention is a promising treatment for PE caused by abnormal placental development. The ability of CMIP upregulation to reduce the clinical symptoms of PE can be attributed to two fundamental mechanisms: enhancing trophoblast cell invasiveness during early pregnancy, modulating the maternal vascular system, and ameliorating abnormal endothelial function. Investigating the in vivo mechanisms of PE and identifying more effective therapeutic methods for this disease are critical.

The documented species-specific subcellular distribution of PDE7B-membrane-associated colocalization with CMIP in human trophoblasts versus predominant nuclear localization in rat placental tissue-may reflect divergent vesicular trafficking mechanisms governing secretory protein compartmentalization between primates and rodents [57, 58]. While CMIP's conserved membrane localization across species underscores its fundamental role in cytoskeletal regulation, PDE7B's nuclear accumulation in rodents could represent transient storage prior to secretion or membrane-independent regulatory functions, a phenomenon consistent with the dual localization patterns documented

for other secreted proteins [59]. Notably, functional analyses demonstrating conserved CMIP-PDE7B coordination in blood pressure modulation and placental development (Fig. 6) suggest that their pathophysiological interaction operates through spatial distribution-independent mechanisms, potentially involving paracrine signaling. Ongoing comparative studies of protein trafficking across placental models will further elucidate these interspecies variations.

The observed disparity between increased blood pressure and complete embryonic loss in the L-NAME+AAV-CON group compared with the L-NAME alone group may result from synergistic interactions between pharmacological and viral stressors. While L-NAME-induced nitric oxide deficiency drives acute hypertension, AAV-CON likely exacerbates systemic inflammation through innate immune activation and causes progressive placental toxicity via particle accumulation or trophoblast dysfunction. This combination amplifies maternal vascular damage while overwhelming embryonic tolerance thresholds, as evidenced by the single surviving fetus. The temporal divergence between acute hemodynamic effects (blood pressure) and cumulative placental compromise (embryo loss) suggests that AAV-CON introduces distinct pathogenic mechanisms, potentially involving sustained angiogenic imbalance or cellular stress responses, that interact critically with the effects of L-NAME. Although adenoviral vectors appear to accentuate specific preeclampsia features, further studies profiling placental vector distribution and cytokine dynamics are needed to delineate these synergistic pathways.

In addition to the sample size, we are aware of various potential confounding factors that are difficult to control and may influence the study's findings. These factors include age [60], prepregnancy body mass index (BMI) [61], prepregnancy lifestyle [62], prepregnancy medical history, and PE prophylaxis use [63]. The complex effects and individual variability of these factors may have affected our findings. Furthermore, we acknowledge that the animal model of PE used in our study, while practical, can not fully replicate the disease itself and that the adenoviral vector given to rats to upregulate CMIP was administered systemically via tail vein injection and did not exclusively target placental trophoblasts. Therefore, it is necessary to validate our findings through further cohort studies and animal studies that employ methods specifically targeting placental trophoblasts.

In conclusion, our study demonstrated that hypoxia-induced CMIP downregulation in placental trophoblasts contributes to trophoblast dysfunction in preeclampsia. Importantly, in vivo administration of exogenous CMIP ameliorated hypertension and improved placental and fetal parameters in a rat model of preeclampsia. These findings offer valuable insights into the underlying mechanisms of PE. Further investigation is needed to elucidate the specific mechanism by which CMIP modulates hypertension in PE and to explore the potential of CMIP as a novel target for PE treatment. Our study lays the groundwork for future research and suggests that our target genes, through a combination of cohort studies, validation via many clinical samples, and clinical applications, may contribute to the development of new drugs or therapeutic approaches for PE patients.

Supplementary Information The online version contains supplementary material available at https://doi.org/10.1007/s00018-025-05726-5.

Author contributions ZLL conceived the study, designed the experiments, and interpreted the data. LYN, YXJ, and YHY performed the experiments with the help of ZYB, GYR, ZXY, YYJ, DYN, SQQ, FY, DHM, YEW, and ZX. ZLL and LYN analyzed/discussed the results and contributed to the manuscript's writing and editing. ZLL and LYN wrote the manuscript. All the authors read and approved the final manuscript.

Funding Henan Province Medical Science and Technology Research (SBGJ202101020, SBGJ202302085, SBGJ202302081), Henan Provincial Science and Technology Research and Development Joint Fund (235200810033).

Data availability The datasets used and analyzed during the current study are available from the corresponding author upon reasonable request.

Declarations

Ethics approval and consent to participate This study was approved by the Ethics Committee of the Third Affiliated Hospital of Zhengzhou University, China (approval number: 2022-338-01) and conducted in accordance with the Declaration of Helsinki. Signed informed consent was obtained from all the study participants. All the experimental processes involving animal treatments were conducted in accordance with the procedures of the Ethical Committee for Animal Experimentation, Zhengzhou University (approval number: ZZU-LAC20230210 [07]).

Consent to participate Not applicable.

Consent for publication All the authors consent to the publication of this study.

Competing interests The authors declare that they have no competing interests.

References

1. Poon LC, Shennan A, Hyett JA, Kapur A, Hadar E, Divakar H et al (2019) The international federation of gynecology and obstetrics (FIGO) initiative on pre-eclampsia: A pragmatic guide for first-trimester screening and prevention. Int J Gynaecol Obstet 145(1):1–33. https://doi.org/10.1002/ijgo.12802
2. Dimitriadis E, Rolnik DL, Zhou W, Estrada-Gutierrez G, Koga K, Francisco RPV et al (2023) Pre-eclampsia. Nat Rev Dis Primers 9(1):8. https://doi.org/10.1038/s41572-023-00417-6
3. Ives CW, Sinkey R, Rajapreyar I, Tita ATN, Oparil S (2020) Preeclampsia-Pathophysiology and clinical presentations: JACC State-of-the-Art review. J Am Coll Cardiol 76(14):1690–1702. https://doi.org/10.1016/j.jacc.2020.08.014
4. Xu Y, Sui L, Qiu B, Yin X, Liu J, Zhang X (2019) ANXA4 promotes trophoblast invasion via the PI3K/Akt/eNOS pathway in preeclampsia. Am J Physiol Cell Physiol 316(4):C481–C91. https://doi.org/10.1152/ajpcell.00404.2018
5. Wei XH, Liao LY, Yin YX, Xu Q, Xie SS, Liu M et al (2024) Overexpression of long noncoding RNA DUXAP8 inhibits ER-phagy through activating AKT/mTOR signaling and contributes to preeclampsia. Cell Mol Life Sci 81(1):336. https://doi.org/10.1007/s00018-024-05385-y
6. Zhang L, Sang M, Li Y, Li Y, Yuan E, Yang L et al (2021) WNT3 hypomethylation counteracts low activity of the Wnt signaling pathway in the placenta of preeclampsia. Cell Mol Life Sci 78(21–22):6995–7008. https://doi.org/10.1007/s00018-021-03941-4
7. Kim S, Shim S, Kwon J, Ryoo S, Byeon J, Hong J et al (2024) Alleviation of preeclampsia-like symptoms through PlGF and eNOS regulation by hypoxia- and NF-kappaB-responsive miR-214-3p deletion. Exp Mol Med 56(6):1388–1400. https://doi.org/10.1038/s12276-024-01237-8
8. Li Y, Cui S, Shi W, Yang B, Yuan Y, Yan S et al (2020) Differential placental methylation in preeclampsia, preterm and term pregnancies. Placenta 93:56–63. https://doi.org/10.1016/j.placenta.2020.02.009
9. Wang T, Xiang Y, Zhou X, Zheng X, Zhang H, Zhang X et al (2019) Epigenome-wide association data implicate fetal/maternal adaptations contributing to clinical outcomes in preeclampsia. Epigenomics 11(9):1003–1019. https://doi.org/10.2217/epi-2019-0065
10. Almomani SN, Alsaleh AA, Weeks RJ, Chatterjee A, Day RC, Honda I et al (2021) Identification and validation of DNA methylation changes in pre-eclampsia. Placenta 110:16–23. https://doi.org/10.1016/j.placenta.2021.05.005
11. Grimbert P, Valanciute A, Audard V, Pawlak A, Le gouvelo S, Lang P et al (2003) Truncation of C-mip (Tc-mip), a new proximal signaling protein, induces c-maf Th2 transcription factor and cytoskeleton reorganization. J Exp Med 198(5):797–807. https://doi.org/10.1084/jem.20030566
12. Ollero M, Sahali D (2021) The enigmatic emerging role of the C-Maf inducing protein in Cancer. Diagnostics (Basel) 11(4). https://doi.org/10.3390/diagnostics11040666
13. Zhang SY, Kamal M, Dahan K, Pawlak A, Ory V, Desvaux D et al (2010) c-mip impairs podocyte proximal signaling and induces heavy proteinuria. Sci Signal 3(122):ra39. https://doi.org/10.1126/scisignal.2000678
14. Yu L, Lin Q, Feng J, Dong X, Chen W, Liu Q et al (2013) Inhibition of nephrin activation by c-mip through Csk-Cbp-Fyn axis plays a critical role in angiotensin II-induced podocyte damage. Cell Signal 25(3):581–588. https://doi.org/10.1016/j.cellsig.2012.11.017
15. Oniszczuk J, Sendeyo K, Chhuon C, Savas B, Cogne E, Vachin P et al (2020) CMIP is a negative regulator of T cell signaling. Cell Mol Immunol 17(10):1026–1041. https://doi.org/10.1038/s41423-019-0266-5
16. Audard V, Zhang SY, Copie-Bergman C, Rucker-Martin C, Ory V, Candelier M et al (2010) Occurrence of minimal change nephrotic syndrome in classical hodgkin lymphoma is closely related to the induction of c-mip in hodgkin-Reed Sternberg cells and podocytes. Blood 115(18):3756–3762. https://doi.org/10.1182/blood-2009-11-251132
17. Zhang J, Huang J, Wang X, Chen W, Tang Q, Fang M et al (2017) CMIP is oncogenic in human gastric cancer cells. Mol Med Rep 16(5):7277–7286. https://doi.org/10.3892/mmr.2017.7541
18. Wang B, Wu ZS, Wu Q (2017) CMIP promotes proliferation and metastasis in human glioma. Biomed Res Int 2017:5340160. https://doi.org/10.1155/2017/5340160
19. Wang CCN, Li CY, Cai JH, Sheu PC, Tsai JJP, Wu MY et al (2019) Identification of prognostic candidate genes in breast Cancer by integrated bioinformatic analysis. J Clin Med 8(8). https://doi.org/10.3390/jcm8081160
20. Kohler PO, Bridson WE (1971) Isolation of hormone-producing clonal lines of human choriocarcinoma. J Clin Endocrinol Metab 32(5):683–687. https://doi.org/10.1210/jcem-32-5-683
21. Gershon E, Maimon I, Galiani D, Elbaz M, Karasenti S, Dekel N (2019) High cGMP and low PDE3A activity are associated with oocyte meiotic incompetence. Cell Cycle 18(20):2629–2640. https://doi.org/10.1080/15384101.2019.1652472
22. Hetman JM, Soderling SH, Glavas NA, Beavo JA (2000) Cloning and characterization of PDE7B, a cAMP-specific phosphodiesterase. Proc Natl Acad Sci U S A 97(1):472–476. https://doi.org/10.1073/pnas.97.1.472
23. Gardner C, Robas N, Cawkill D, Fidock M (2000) Cloning and characterization of the human and mouse PDE7B, a novel cAMP-specific Cyclic nucleotide phosphodiesterase. Biochem Biophys Res Commun 272(1):186–192. https://doi.org/10.1006/bbrc.2000.2743
24. Veerbeek JH, Brouwers L, Koster MP, Koenen SV, van Vliet EO, Nikkels PG et al (2016) Spiral artery remodeling and maternal cardiovascular risk: the spiral artery remodeling (SPAR) study. J Hypertens 34(8):1570–1577. https://doi.org/10.1097/HJH.0000000000000964
25. Chiang YT, Seow KM, Chen KH (2024) The pathophysiological, genetic, and hormonal changes in preeclampsia: A systematic review of the molecular mechanisms. Int J Mol Sci 25(8). https://doi.org/10.3390/ijms25084532
26. Rana S, Lemoine E, Granger JP, Karumanchi SA, Preeclampsia (2019) Pathophysiology, challenges, and perspectives. Circ Res 124(7):1094–1112. https://doi.org/10.1161/CIRCRESAHA.118.313276
27. Grimbert P, Valanciute A, Audard V, Lang P, Guellaen G, Sahali D (2004) The Filamin-A is a partner of Tc-mip, a new adapter protein involved in c-maf-dependent Th2 signaling pathway. Mol Immunol 40(17):1257–1261. https://doi.org/10.1016/j.molimm.2003.11.035
28. Li H, Peng H, Hong W, Wei Y, Tian H, Huang X et al (2022) Human placental endothelial cell and trophoblast heterogeneity and differentiation revealed by Single-Cell RNA sequencing. Cells 12(1). https://doi.org/10.3390/cells12010087
29. Arutyunyan A, Roberts K, Troule K, Wong FCK, Sheridan MA, Kats I et al (2023) Spatial multiomics map of trophoblast development in early pregnancy. Nature 616(7955):143–151. https://doi.org/10.1038/s41586-023-05869-0

30. Sahali D, Pawlak A, Valanciute A, Grimbert P, Lang P, Remy P et al (2002) A novel approach to investigation of the pathogenesis of active minimal-change nephrotic syndrome using subtracted cDNA library screening. J Am Soc Nephrol 13(5):1238–1247. https://doi.org/10.1681/ASN.V1351238
31. Omori K, Kotera J (2007) Overview of PDEs and their regulation. Circ Res 100(3):309–327. https://doi.org/10.1161/01.RES.0000256354.95791.f1
32. Crocetti L, Floresta G, Cilibrizzi A, Giovannoni MP (2022) An overview of PDE4 inhibitors in clinical trials: 2010 to early 2022. Molecules 27(15). https://doi.org/10.3390/molecules27154964
33. Zorn A, Baillie G (2023) Phosphodiesterase 7 as a therapeutic target - Where are we now? Cell Signal 108:110689. https://doi.org/10.1016/j.cellsig.2023.110689
34. Kelly MP (2018) Cyclic nucleotide signaling changes associated with normal aging and age-related diseases of the brain. Cell Signal 42:281–291. https://doi.org/10.1016/j.cellsig.2017.11.004
35. Morales-Garcia JA, Palomo V, Redondo M, Alonso-Gil S, Gil C, Martinez A et al (2014) Crosstalk between phosphodiesterase 7 and glycogen synthase kinase-3: two relevant therapeutic targets for neurological disorders. ACS Chem Neurosci 5(3):194–204. https://doi.org/10.1021/cn400166d
36. Duan FM, Fu LJ, Wang YH, Adu-Gyamfi EA, Ruan LL, Xu ZW et al (2021) THBS1 regulates trophoblast fusion through a CD36-dependent Inhibition of cAMP, and its upregulation participates in preeclampsia. Genes Dis 8(3):353–363. https://doi.org/10.1016/j.gendis.2020.05.007
37. Sun C, Mei J, Yi H, Song M, Ma Y, Huang Y (2024) The effect of the cAMP signaling pathway on HTR8/SV-Neo cell line proliferation, invasion, and migration after treatment with forskolin. Reprod Sci 31(5):1268–1277. https://doi.org/10.1007/s43032-023-01396-5
38. Jin X, Mao L, Zhao W, Liu L, Li Y, Li D et al (2022) Decidualization-derived cAMP promotes decidual NK cells to be angiogenic phenotype. Am J Reprod Immunol 88(3):e13540. https://doi.org/10.1111/aji.13540
39. Sassone-Corsi P (2012) The Cyclic AMP pathway. Cold Spring Harb Perspect Biol 4(12). https://doi.org/10.1101/cshperspect.a011148
40. Zhang H, Kong Q, Wang J, Jiang Y, Hua H (2020) Complex roles of cAMP-PKA-CREB signaling in cancer. Exp Hematol Oncol 9(1):32. https://doi.org/10.1186/s40164-020-00191-1
41. Takahashi T, Shibasaki T, Takahashi H, Sugawara K, Ono A, Inoue N et al (2013) Antidiabetic sulfonylureas and cAMP cooperatively activate Epac2A. Sci Signal 6(298):ra94. https://doi.org/10.1126/scisignal.2004581
42. Yarwood SJ, Steele MR, Scotland G, Houslay MD, Bolger GB (1999) The RACK1 signaling scaffold protein selectively interacts with the cAMP-specific phosphodiesterase PDE4D5 isoform. J Biol Chem 274(21):14909–14917. https://doi.org/10.1074/jbc.274.21.14909
43. Bender AT, Beavo JA (2006) Cyclic nucleotide phosphodiesterases: molecular regulation to clinical use. Pharmacol Rev 58(3):488–520. https://doi.org/10.1124/pr.58.3.5
44. Dodge-Kafka KL, Soughayer J, Pare GC, Carlisle Michel JJ, Langeberg LK, Kapiloff MS et al (2005) The protein kinase A anchoring protein mAKAP coordinates two integrated cAMP effector pathways. Nature 437(7058):574–578. https://doi.org/10.1038/nature03966
45. Pfleger KD, Eidne KA (2006) Illuminating insights into protein-protein interactions using bioluminescence resonance energy transfer (BRET). Nat Methods 3(3):165–174. https://doi.org/10.1038/nmeth841
46. Plantenberg JH, de Groot PC, Harmans CJ, Mooij JE (2007) Demonstration of controlled-NOT quantum gates on a pair of superconducting quantum Bits. Nature 447(7146):836–839. https://doi.org/10.1038/nature05896
47. Saadeldin IM, Kim SJ, Choi YB, Lee BC (2014) Post-maturation Zona perforation improves Porcine parthenogenetic trophoblast culture. Placenta 35(4):286–288. https://doi.org/10.1016/j.placenta.2014.02.003
48. Oh SY, Chu T, Sadovsky Y (2011) The timing and duration of hypoxia determine gene expression patterns in cultured human trophoblasts. Placenta 32(12):1004–1009. https://doi.org/10.1016/j.placenta.2011.09.010
49. Zhao H, Wong RJ, Stevenson DK (2021) The impact of hypoxia in early pregnancy on placental cells. Int J Mol Sci 22(18). https://doi.org/10.3390/ijms22189675
50. Yan X, Fang Y, Yuan Y, Ding Y, Yu H, Li Y et al (2024) Combined analysis of the effects of hypoxia and oxidative stress on DNA methylation and the transcriptome in HTR-8/SVneo trophoblast cells. J Cell Mol Med 28(12):e18469. https://doi.org/10.1111/jcmm.18469
51. Shigemitsu A, Naruse K, Kobayashi H (2022) Hypoxia promotes extravillous trophoblast cell invasion through the Hypoxia-Inducible factor Urokinase-Type plasminogen activator receptor pathway. Gynecol Obstet Invest 87(3–4):232–241. https://doi.org/10.1159/000525851
52. Zhu J, Wang K, Li T, Chen J, Xie D, Chang X et al (2017) Hypoxia-induced TET1 facilitates trophoblast cell migration and invasion through HIF1alpha signaling pathway. Sci Rep 7(1):8077. https://doi.org/10.1038/s41598-017-07560-7
53. Ma F, Feng X, Feng S, Liu J, Li J, Mo L et al (2024) Impaired inducibility of immune regulatory capacity of peripheral B cells of patients with recurrent pregnancy loss. Immunol Res 72(6):1502–1514. https://doi.org/10.1007/s12026-024-09549-7
54. Xu X, Mo L, Liao Y, Zhang KS, Zhang H, Liu L et al (2024) An association between elevated telomerase reverse transcriptase expression and the immune tolerance disruption of dendritic cells. Cell Commun Signal 22(1):284. https://doi.org/10.1186/s12964-024-01650-6
55. Ron D, Walter P (2007) Signal integration in the Endoplasmic reticulum unfolded protein response. Nat Rev Mol Cell Biol 8(7):519–529. https://doi.org/10.1038/nrm2199
56. Buhimschi IA, Saade GR, Chwalisz K, Garfield RE (1998) The nitric oxide pathway in pre-eclampsia: pathophysiological implications. Hum Reprod Update 4(1):25–42. https://doi.org/10.1093/humupd/4.1.25
57. Enders AC, Carter AM (2006) Comparative placentation: some interesting modifications for histotrophic nutrition -- a review. Placenta 27(Suppl A):S11–S16. https://doi.org/10.1016/j.placenta.2005.10.013
58. Harris LK (2010) Review: Trophoblast-vascular cell interactions in early pregnancy: how to remodel a vessel. Placenta 31(Suppl):S93–S98. https://doi.org/10.1016/j.placenta.2009.12.012
59. Nickel W, Rabouille C (2009) Mechanisms of regulated unconventional protein secretion. Nat Rev Mol Cell Biol 10(2):148–155. https://doi.org/10.1038/nrm2617
60. Saccone G, Gragnano E, Ilardi B, Marrone V, Strina I, Venturella R et al (2022) Maternal and perinatal complications according to maternal age: A systematic review and meta-analysis. Int J Gynaecol Obstet 159(1):43–55. https://doi.org/10.1002/ijgo.14100
61. Lee WL, Lee FK, Wang PH (2022) Pre-pregnancy body mass index and outcome of preeclampsia. Taiwan J Obstet Gynecol 61(5):737–738. https://doi.org/10.1016/j.tjog.2022.05.010
62. Yang Y, Le Ray I, Zhu J, Zhang J, Hua J, Reilly M, Preeclampsia, Prevalence (2021) Risk factors, and pregnancy outcomes in Sweden and China. JAMA Netw Open 4(5):e218401. https://doi.org/10.1001/jamanetworkopen.2021.8401

63. Chaiworapongsa T, Chaemsaithong P, Korzeniewski SJ, Yeo L, Romero R (2014) Pre-eclampsia part 2: prediction, prevention and management. Nat Rev Nephrol 10(9):531–540. https://doi.org/10.1038/nrneph.2014.103